Dependence of Positive Binding Energies on Side Chains—A Theoretical Prediction on the Origin of Regular Ordering for the Amino Acid Residues in the Selectivity Filter

Hongqi Ai,*,† Chong Zhang,‡ Yun Li,† Liang Zhang,§ and Fang Li†

School of Chemistry and Chemical Engineering, University of Jinan, Jinan, 250022, People's Republic of China, Department of Chemistry and Technology, Liaocheng University, Liaocheng, 252059, People's Republic of China, and Institute of Theoretical Chemistry, Shandong University, Jinan, 250100, People's Republic of China

Received: May 31, 2007; In Final Form: September 17, 2007

The side-chain effects of metalated and protonated dipeptides, including GGH^+M^+, GAH^+M^+, AGH^+M^+, AAH^+M^+, GWH^+M^+, GSH^+M^+, GTH^+M^+, GFH^+M^+, GYH^+M^+, and GVH^+M^+ (G = glycine, A = alanine, W = tryptophan, S = serine, T = threonine, F = phenylalanine, and V = valine; M = Li, Na, and K), are theoretically explored in this paper on their positive binding energies (PBEs), which are derived from interactions of M^+ with the carboxyl oxygen(s). The B3LYP/6-311++G**// B3LYP/6-31G* calculations suggest that the PBEs of dipeptides with side chain(s) are much smaller than those with no side chain (GGH^+M^+). Generally, larger side chains and smaller M^+ radii would lead to fewer PBEs for the M^+ involved systems. On the basis of the direct dependence of PBE on the electrostatic repulsion between two kinds of cations (H^+ and M^+) in these dipeptide models, it could be reasonably expected that the side-chain effect on the electrostatic repulsion and consequently on the PBEs could offer one good insight, on a chemical−physical basis, into the origin of regular ordering of the amino acids when they form a filter in the K^+ channel protein (MacKinnon, et al. *Science* **1998**, *280,* 106).

1. Introduction

Protonated or metalated amino acids and oligopeptides have been given much attention due to their importance in understanding protein behaviors.[1−15] This is especially true for those peptides with particularly long chains. However, the flexibility of such a long chain generally leads to a very complicated potential energy surface (PES) and, of course, would cost very long computation time.[16] Therefore, for the favor of experimental tractability and computational simplicity, some amino acid molecules and peptides of appropriate size are often selected as models for probing the protein properties of interest, such as the protonation,[1−5] metalation, and so forth.[6−15]

The peptides contain a series of active sites, such as amino nitrogens and carbonyl oxygens in different amino acid residues. They are prone to be readily protonated and metalated. Until now, there have been many papers focusing on the interactions between one of these active sites and a single cation (proton or metal ion) in some amino acids or oligopeptides,[1−15] which provide very meaningful information on the nature of protonated or metalated peptides. Some double-ion coupling phenomena in life were also reported, such as proton pump,[17] Na, K-ATPase,[18] ion channel,[19] Cu^+-bound proton transport,[20] and Ca^{2+}-ATPase[21] transport, etc. Recently, our group has probed the interactions of glycine with H^+, Li^+, and Na^+[22] and observed an interesting phenomenon of positive binding energy (PBE). Namely, the energy sum of two reactant species is lower than that of the product (complex), whereas the frequency calculations confirm that the complex is still a minimum on the PES. The definition of PBE for the $P_2H^+...Mx^+$ complex is as follows:

$$\Delta E = E_C - E_{P_2H}{}^+ - E_M{}^+$$

where E_C, $E_{P_2H}{}^+$, and $E_M{}^+$ (M = Li, Na, and K) denote the energies of $P_2H^+Mx^+$ (product), P_2H^+ (reactant, a protonated dipeptide), and M^+ (reactant), respectively. In our previous work, we found that the PBE mainly derived from the electronic effect[23] of double-ion coupled systems, in which at least one M^+ was involved.[22] The binding energy (or affinity energy) of either proton was negative in the diprotonized glycine systems except for some water-molecule assistant cases.[24] Interestingly, for the double ion-involved (at least a M^+) peptides, such a PBE rule was found to be greatly influenced by the length of the main chains, and its value would become negative when $n \geq 4$ for $G_nH^+Li^+$, $n \geq 5$ for $G_nH^+Na^+$, and $n \geq 6$ for $G_nH^+K^+$ systems.[25] The "*n*" denotes the number of glycine residues (G) between two cations (H^+ and M^+).

The PBE produced by the interaction of multications in the biomolecules, such as two or more K^+ ions coordinating, respectively, to adjacent carboxyl oxygens in the selectivity filter,[19] might be the driving force of biological engines, albeit locally unfavorable for the stability of the system. In this sense, that which is locally unfavorable for the stability is requisite.[26] Many experiments had suggested that not only the main chains could influence the PBEs of peptides, but also the side chains as well.[27] For example, Guidoni and co-workers[26] concluded that the PBE of the K^+−O bond in the KcsA K^+ channel protein was mainly derived from the electrostatic repulsion between different side chain groups.[22−23] Shrivastava et al. reported that the 2−3 K^+ ions permeation through the narrow 12 Å "selectivity filter" maybe related to the breathing motions of

* To whom correspondence should be addressed. E-mail: chm_aihq@ujn.edu.cn.
† University of Jinan.
‡ Liaocheng University.
§ Shandong University.

10.1021/jp074198m CCC: $37.00
Published on Web 11/20/2007

SCHEME 1: Illustration of Selectivity Filter in the K^+ Ion Channel (See Panel a); Panel b Is the Corresponding Model Structure, in Which Only Two-Four Opposite TVGY Residue Chains Are Reserved for Clear Show, and Three K^+ Ions and One Water Molecule Are Buried According to Ref 36

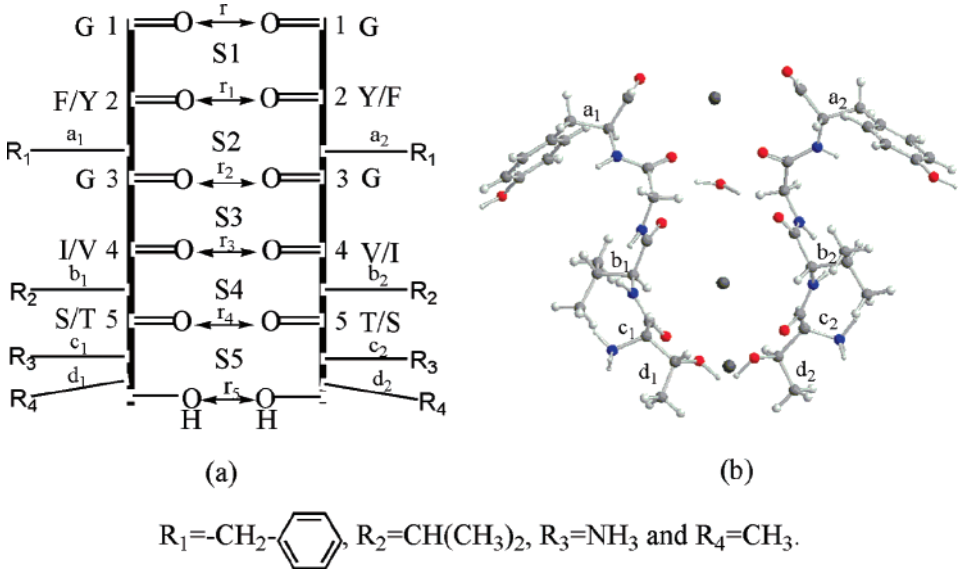

R_1=-CH_2-C_6H_5, R_2=$CH(CH_3)_2$, R_3=NH_3 and R_4=CH_3.

intracellular mouth of the protein.[28] Because the filter is composed of four TVGYG chains[19] (see Scheme 1), the five carboxyl oxygens of each chain are almost in line, and each K^+ ion coordinates eight oxygen atoms to form a multidentate structure, the breathing motion perhaps derives from the different sensitivities on the ion transport or the electrostatic repulsion for the five amino acid residues with different side chains in the TVGYG peptide. MacKinnon et al.[29] have confirmed that the two glycine residues are strictly conserved at the positions of 1 and 3 (S1 and S3) in the selectivity filter over many types of K^+ channels, and the variation of residues at positions 2, 4, and 5 (S2, S4, and S5) is only restricted to between tyrosine (Y) and phenylalanine (F), valine (V) and isoleucine (I), and threonine (T) and serine (S), respectively. The regular ordering of these amino acids indicates that their different side chains must play vital roles, which still remains unclear on the chemical and physical basis.[30]

For this purpose, the interactions of M^+ (Li^+, Na^+, K^+) with protonated dipeptides with different side chains [Gly-Gly+H^+ (GGH^+), Gly-Ala+H^+ (GAH^+), Ala-Gly+H^+ (AGH^+), Ala-Ala+H^+ (AAH^+), and Gly-Trp+H^+ (GWH^+)], whose structural information is derived from refs 3, 5, 10, and 15, together with the PBEs of these reactions, will be theoretically explored in this work. Because the side chains in these dipeptides (from GGH^+, GAH^+,..., to GWH^+) are gradually enlarged in size, the PBE dependence on the size of these different side chains should be very interesting. For each of these protonated dipeptides, the most optimal M^+ complex should be discovered if we let the M^+ match with one of its two bare carboxyl oxygens (C)O.

In addition, on the basis of the knowledge of the obtained PBEs' dependence on the size of different side chains, further attempts are made to illuminate the regular ordering of the TVGYG chain, in which the additional dipeptides—GSH^+Na^+/K^+, GTH^+Na^+/K^+, GYH^+Na^+/K^+, GFH^+Na^+/K^+, and GVH^+-Na^+/K^+ are employed as models. To explore the PBE effect on the K^+ ions transport in the selectivity filter, the $P_2H^+Mx^+$, rather than $P_2K^+Mx^+$, is selected as model in this work for the following considerations: (1) The PBE of M^+ in $P_2H^+Mx^+$ is larger than that in $P_2K^+Mx^+$,[22]and thus the PBE dependence on the side chains in the $P_2H^+Mx^+$ system can be observed more obviously. (2) Previous studies had revealed that the protonation at the amino terminal of the peptides could hardly induce the deformation of the corresponding main chain,[1−5] whereas the metalation at any site(s) of the peptides could.[6−15] Simultaneously, it is requisite to employ the peptides with linear (extended) structures to analogy each TVGYG chain in the filter, which also has almost linear display of its five carboxyl oxygens.[19] Moreover, the nearly linear peptide with protonation at its amino terminal is almost the most stable one compared with other shaped peptides.[1−5] (3) Protonation at the amino terminal of the peptides can reserve all of the bare carboxyl oxygens to match with M^+ freely, which gives us computational and comparative convenience.

2. Calculation Schemes

For the reactions of $P_2H^+ + M^+ \rightarrow P_2H^+Mx^+$, two kinds of $P_2H^+Mx^+$ complexes ($P_2H^+M1^+$ and $P_2H^+M2^+$) should be produced when one M^+ attacks the bare carboxyl oxygens of P_2H^+ species, respectively.[3,5] Each $P_2H^+Mx^+$ isomer has one PBE value.[25]

Because the hybrid density functional theory (DFT) can give very similar structural parameters compared with the MP2, and density functional vibrational frequencies and intensities are in excellent agreement with the experimental data for amino acid systems[31] and similar systems,[32] the B3LYP/6-311++G**// B3LYP/ 6-31G* calculation[33] is employed in this work (unless those specially specified). The zero point vibrational energy (ZPVE) corrections and basis set superposition error (BSSE)[34] corrections are also performed at the same level in order to gain more precision. These calculations are carried out with GAUSSIAN 03 program, Revision C.02.[35]

Molecular dynamics (MD) is computed for the model of KcsA K^+ channel protein, in which only the structure composed of four equal TVGYG chains is considered and the outer linkage sites of the model are saturated by hydrogens. No lipidic or water environment constitutive of the MD construct is considered. The geometry of this model is truncated from the crystal structure of the KcsA K^+ channel[19] (Protein Data Bank (PDB)[36] accession number 1BL8). Due to the similar structural character of the top G and middle G in the TVGYG chain, the simplified

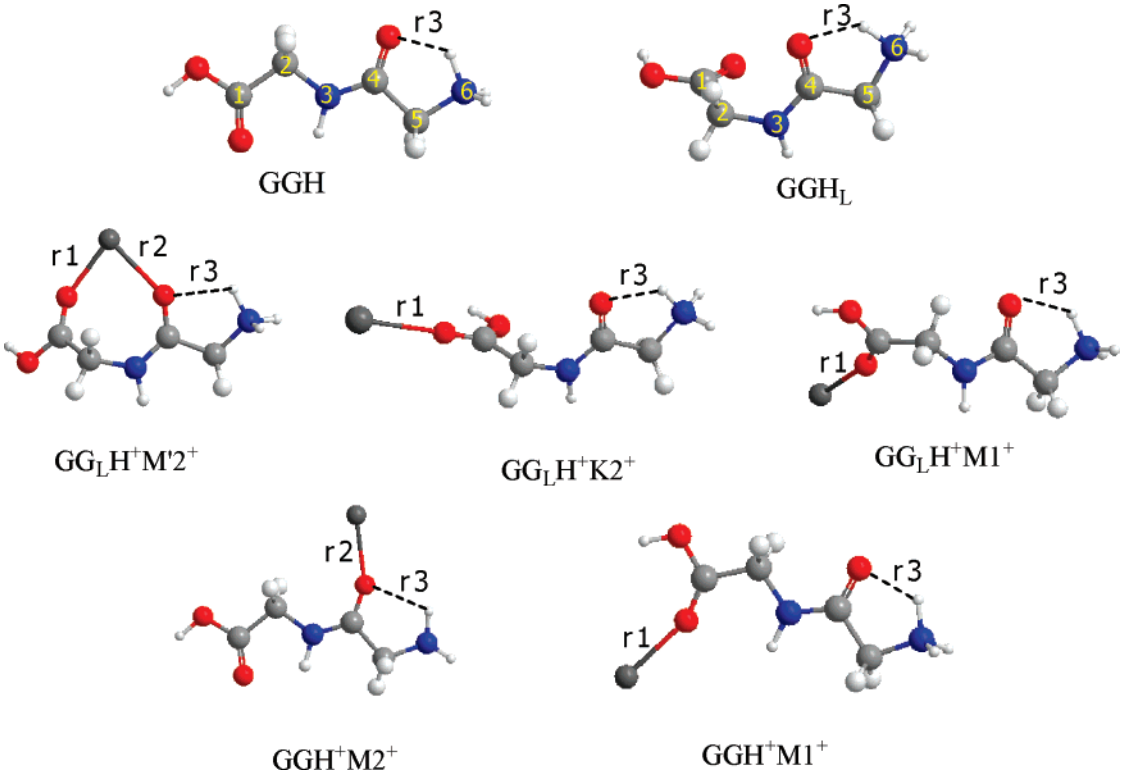

Figure 1. B3LYP/6-31G*-optimized structures of $GG_{(L)}H^+Mx^+$ ($M^+ = M^+ + K^+ = Li^+, Na^+, K^+$; $x = 1$ or 2) and their reactants $GG_{(L)}H^+$. Those geometries, which change drastically and cannot be denoted by the general form $GG_{(L)}H^+Mx^+$, are shown separately with the specified M^+. Hydrogen bonding in broken line. Distance in angstrom.

model (model1) composed of four equal TVGY chains is simulated herein for time-saving reason. Such simplification is proved to be feasible by Compoint et al.[37] Obviously, a full quantum computation on all of the atoms of the system plus a real or modeled lipidic and aqueous environment would, of course, be ideal for an accurate description of the selectivity filter, but it would be unconceivable for current computational level (see the following).

The time step and total time of simulation are 1 fs and 1000 fs, respectively. The neighboring list is updated every 10 steps under NVE and $T = 298.0$ K conditions. The SCF tolerance is 10^{-4}. All of the simulations employ the PWC[38] exchange-correlation functional and double-numeric quality (DN) basis set implemented in the DFT program package $D_{MOL}{}^3$.[39] The DN basis set is smaller and less accurate than the DND (DN plus *d*-functions for all atoms but H) and the DNP (DND plus *p*-functions for H atom) basis sets, but capable of qualitatively describing the electronic properties of the model1.[40] Moreover, it is impractical to carry out MD computations for such system as model1 by using the DND or DNP basis set. Thus the DN basis set is employed in the subsequent MD simulations for our computational facility.

3. Results and Discussion

3.1. Geometries and Relative Stabilities of $P_2H^+Mx^+$ and P_2H^+. The structures of P_2H^+ (reactants), together with its M^+-coupled complex named as $P_2H^+Mx^+$ (products), are depicted in Figure 1 and Figures 1S−4S, respectively. As a representative, Figure 1 is presented in the text (see Supporting Information). In these figures, the atoms of main chain of P_2H^+ are numbered as i ($i = 1, 2, ..., 6$) and in the text, the suffixed numbers are the corresponding atoms. The corresponding atoms in their metalated complexes ($P_2H^+Mx^+$) also have same meanings (not shown). The characteristic parameters of $P_2H^+Mx^+$ and P_2H^+ are listed in Table 1, including the $M^+-O(C_{1,4})$ distances, $(N_6)H^+...O(C_4)$ hydrogen bond distances and dihedral angles $\tau(C_1C_2N_3C_4)$. Generally, the metalation at any carboxyl oxygen of P_2H^+ would induce the distortion of its main chains, which can be reflected by the dihedral angle changes before and after M^+ coupling with P_2H^+. For convenience, only the $\tau(C_1C_2N_3C_4)$ is discussed in this paper due to its most remarkable change relative to other dihedral angles.

3.2. $GG_{(L)}H^+Mx^+$. As in refs 2−4, the stable protonated GG dipeptides include the linear GGH^+ and L GG_LH^+, respectively. Both of them are protonated at their terminal nitrogens (see Figure 1). The main chain dihedral angles of the C-terminal $\tau(C_1C_2N_3C_4)$, the N-terminal $\phi(N_6C_5C_4N_3)$, and peptide bond $\psi(C_2C_3N_4C_5)$ in the linear GGH^+ are 180.0°, 180.0°, and 180.0°, respectively.[3,5] The main difference of GG_LH^+ structure compared with GGH^+ is the τ, which is 75.4° (76.3° from ref 3-*A2e* obtained at the B3LYP/6-31G* level and 66.5° from ref 5 at the MP2/6-311++G** level). In the GG_LH^+, the contorted dihedral angle causes the array of its main chain like a "L"-shape. Previous investigations[2−4] revealed that the GG_LH^+ was larger in energy (2.01 kcal/mol from ref 3) than the linear GGH^+.[3,4] However, since the M^+ metalation with GG_LH^+ could produce stable bidentate metal complexes more easily than with the linear GGH^+ due to the structural preponderance of the former (without suffering great deformation), the M^+ metalation of GGH^+ and GG_LH^+ are both discussed in this section.

As expected, most metalated structures are derived from the protonated L dipeptides. Because there are two bare carboxyl oxygens, respectively, in the two different shape dipeptides (GGH^+/GG_LH^+), there may be four metalated complexes obtained after metalation with M^+ (Figure 1), and their relative energies are shown in Table 2. The data in Table 2 suggest that the $GG_LH^+M2^+$ is the most stable structure among all isomers except for the $GG_LH^+Na2^+$. For the sodium ion-involved

TABLE 1: B3LYP/6-31G*-Optimized Characteristic Parameters of These Protonated and Metalated Dipeptides with Different Side Chains[a]

complex	r1	r2	r3	$\tau(C_1C_2N_3C_4)$	complex	r1	r2	r3	τ ($C_1C_2N_3C_4$)
GG_LH^+			1.726	76.4	GA_LH^+			1.715	−73.1
$GG_LH^+Li2^+$	1.852	1.934	2.143	73.8	$GA_LH^+Li2^+$	1.853	1.933	2.117	−74.5
$GG_LH^+Na2^+$	2.210	2.385	2.075	77.8	$GA_LH^+Na2^+$	2.207	2.388	2.042	−76.9
$GG_LH^+K2^+$	2.644		1.825	94.8	$GA_LH^+K2^+$	2.632		1.815	−81.5
$GG_LH^+Li1^+$	1.812		1.853	111.7	$GA_LH^+Li1^+$	1.800		1.862	−72.2
$GG_LH^+Na1^+$	2.204		1.838	115.9	$GA_LH^+Na1^+$	2.187		1.837	−76.3
$GG_LH^+K1^+$	2.701		1.802	140.2	$GA_LH^+K1^+$	2.640		1.804	−123.8
GGH^+			1.711	180.0	GAH^+			1.702	−163.3
GGH^+Li2^+		1.827	2.337	180.0	GAH^+Li2^+		1.822	2.318	−162.2
GGH^+Na2^+		2.247	2.188	180.0	GAH^+Na2^+		2.238	2.166	−162.3
GGH^+K2^+		2.802	2.026	−179.3	GAH^+K2^+		No		
GGH^+Li1^+	1.833		1.823	179.5	GAH^+Li1^+	1.800		1.862	−72.3
GGH^+Na1^+	2.231		1.806	179.9	GAH^+Na1^+	2.187		1.837	−75.9
GGH^+K1^+	2.730		1.789	180.0	GAH^+K1^+	2.701		1.782	−152.8
AA_LH^+			1.751	−74.1	AGH^+			1.710	−179.8
$AA_LH^+Li2^+$	1.855	1.921	2.152	−74.8	AGH^+Li2^+		1.819	2.361	179.9
$AA_LH^+Na2^+$	2.210	2.364	2.091	−77.2	AGH^+Na2^+		2.232	2.224	179.6
$AA_LH^+K2^+$	2.627		1.842	−81.7	AGH^+K2^+		2.764	2.078	179.2
$AA_LH^+Li1^+$	1.797		1.897	−67.8	AGH^+Li1^+	1.808		1.852	105.2
$AA_LH^+Na1^+$	2.183		1.864	−71.3	AGH^+Na1^+	2.199		1.828	109.2
$AA_LH^+K1^+$	2.627		1.842	−81.7	AGH^+K1^+	2.723		1.804	172.9
AAH^+			1.700	−162.1	GWH^+			1.927	−151.9
AAH^+Li2^+		1.814	2.334	−161.2	GWH^+Li2^+		1.864	2.329	−153.1
AAH^+Na2^+		2.226	2.203	−160.7	GWH^+Na2^+		2.222	2.319	−151.9
AAH^+K2^+		2.752	2.060	−160.9	GWH^+K2^+		2.641	2.273	−150.5
$A_2H^+Li1^+$	1.802		1.880	−68.5	GWH^+Li1^+	1.798		2.044	−140.7
AAH^+Na1^+	2.181		1.869	−72.9	GWH^+Na1^+	2.185		2.025	−142.4
AAH^+K1^+	2.630		1.845	−86.7	GWH^+K1^+	2.638		2.005	−144.4
GSH^+			1.688	−143.7	GFH^+			1.690	−61.8
GSH^+Na1^+	2.189		1.817	−132.1	GFH^+Na1^+	2.171		1.829	−62.8
GSH^+K1^+	2.645		1.799	−135.1	GFH^+K1^+	2.613		1.811	−62.3
GTH^+			1.683	−145.4	GYH^+			1.689	−60.5
GTH^+Na1^+	2.177		1.846	−60.6	GYH^+Na1^+	2.168		1.825	−61.7
GTH^+K1^+	2.614		1.814	−53.8	GYH^+K1^+	2.606		1.808	−60.8
GVH^+			1.697	−136.6					
GVH^+Na1^+	2.175		1.828	−70.1					
GVH^+K1^+	2.611		1.812	−74.7					

[a] Distances are in angstroms.

TABLE 2: ZPVE-Corrected Relative Energies of These Protonated and Metalated Dipeptides with Different Side Chains from (I) B3LYP/6-31G* and (II) B3LYP/ 6-311++G//6-31G*, Respectively[a]**

complex	I	II	complex	I	II	complex	I	II
$GG_LH^+Li2^+$	0	0	$GG_LH^+Na2^+$	0	0	$GG_LH^+K2^+$	0	0
$GG_LH^+Li1^+$	6.0	3.5	$GG_LH^+Na1^+$	0.8	−1.1	$GG_LH^+K1^+$	6.0	6.1
GGH^+Li2^+	6.9	4.6	GGH^+Na2^+	0.9	−0.9	GGH^+K2^+	5.6	5.8
GGH^+Li1^+	17.8	15.7	GGH^+Na1^+	11.9	10.2	GGH^+K1^+	16.0	16.5
$G_LAH^+Li2^+$	0	0	$GA_LH^+Na2^+$	0	0	$GA_LH^+K2^+$	0	0
AGH^+Li1^+	6.2	3.8	AGH^+Na1^+	0.8	−1.0	AGH^+K1^+	4.1	4.2
GAH^+Li1^+	7.0	4.8	GAH^+Na1^+	1.9	0.2	GAH^+K1^+	0	0
$GA_LH^+Li1^+$	7.0	4.8	$GA_LH^+Na1^+$	1.9	0.2	$GA_LH^+K1^+$	0.1	0.2
AGH^+Li2^+	16.3	14.1	AGH^+Na2^+	10.6	8.9	AGH^+K2^+	13.1	13.4
GAH^+Li2^+	19.6	17.6	GAH^+Na2^+	13.7	12.2	GAH^+K2^+	no	
$AA_LH^+Li2^+$	0	0	AAH^+Na1^+	0	0	$AA_LH^+K1^+$	0	0
AAH^+Li1^+	3.2	1.0	$AA_LH^+Na2^+$	2.4	4.2	AAH^+K1^+	0	0
$AA_LH^+Li1^+$	8.4	6.3	$AA_LH^+Na1^+$	5.6	5.8	$AA_LH^+K2^+$	0.1	0.1
AAH^+Li2^+	19.3	17.2	AAH^+Na2^+	16.0	16.2	AAH^+K2^+	15.2	15.7
GWH^+Li2^+	0	0	GWH^+Na1^+	0	0	GWH^+K1^+	0	0
GWH^+Li1^+	5.2	2.1	GWH^+Na2^+	1.8	4.2	GWH^+K2^+	6.4	7.8

[a] Energy in kcal/mol.

systems, monodentate $GG_LH^+Na1^+$ becomes the most stable structure and $GG_LH^+Na2^+$ concedes to the third most stable one. Due to the smaller ion radii and more charge distributions of Li^+ and Na^+, both $GG_LH^+Li2^+$ and $GG_LH^+Na2^+$ are bidentate structures, whereas the $GG_LH^+K2^+$ is a monodentate one. The second most stable structures are very different for the three different metal ion-involved systems. In detail, the $GG_LH^+Li1^+$, which is a monodentate, is 3.5 kcal/mol less stable than the complex $GG_LH^+Li2^+$, the most stable structure of Li^+-involved bidentate system. For the Na^+-involved systems, results show that the bidentate $GG_LH^+Na2^+$ and the linear monodendate GGH^+Na2^+ are 1.1 and 0.3 kcal/mol higher in energy than the most stable $GG_LH^+Na1^+$, and thus become the third and second most stable isomer, respectively. This may be caused by the longer $H^+...Na^+$ distance in the $GG_LH^+Na1^+$ (7.431 Å) compared with that in the $GG_LH^+Na2^+$ (4.005 Å). In other words, the increase of electrostatic repulsion and deformation is larger than that of the metal−ligand binding strength in

$GG_LH^+Na2^+$ and thereby decreases its stability. The longer $H^+...Na^+$ distance in $GG_LH^+Na1^+$ results in less repulsion and more stability than that of the $GG_LH^+Na2^+$ counterpart. For the K^+ involved systems, the energies of GGH^+K2^+ and $GG_LH^+K1^+$ are 5.8 and 6.1 kcal/ mol, respectively, less stable than the $GG_LH^+K2^+$ complex, which is the most stable K^+ coupling complex for its longer K^+-O distance (2.644 Å), less charge distribution of K^+, and shorter $(N_6)H...O(C_4)$ hydrogen bond (1.825 Å), respectively.

3.3. $GA_{(L)}H^+Mx^+$ and $AG_{(L)}H^+Mx^+$. After protonation at the terminal nitrogen (N_6) and metalation at each bare carboxyl oxygen ($C_{1\text{ or }4}$)−O of GA_L, GA and AG,[5] six different isomers ($GA_LH^+M1^+$, $GA_LH^+M2^+$, GAH^+M1^+, GAH^+M2^+, AGH^+M1^+, and AGH^+M2^+) are obtained and displayed in Figure 1S (see Supporting Information).

As shown in Table 2, the most stable isomer of Li^+-involved systems is the five-membered-ring $GA_LH^+Li2^+$, in which both the bidentate coordination between the Li^+ and two carboxyl oxygens and $(C_4)O...H(N_6)$ hydrogen-bonding contribute to stronger stability of the structure. The distance between Li^+ and H^+ is 3.714 Å, shorter than the counterpart in $GA_LH^+Na2^+$, suggesting that the repulsion effect in $GA_LH^+Li2^+$ is stronger, which would reduce its stability in some degree. However, the bidentate Li^+-O coordination can effectively counteract the repulsion and keep the structure most stable among its isomers. Due to the larger ion radii and smaller charge distribution of the Na^+ and K^+,[41] the most stable Na^+/K^+-involved systems degenerate into the monodentate AGH^+Na1^+ and $GA_LH^+K2^+$, respectively. For the former, the dihedral angle $\tau(C_1C_2N_3C_4) = -109.2°$ of the main peptide chain and the distance (7.104 Å) between two ions are almost the largest among its isomers. The methyl side chain in the AGH^+Na1^+ structure is close to the protonated N-terminus, thus greatly decreases the repulsion of two positive charge centers (ions). This is also confirmed by the smallest dipole moment (9.32 Debye) of AGH^+Na1^+ relative to those in other isomers (see Table 1S, the Supporting Information). For the K^+-involved systems, Table 2 reveals that both monodentate $GA_LH^+K2^+$ and GAH^+K1^+ have equivalent energies and are the most stable structures among their isomers. Should the $GA_LH^+K2^+$ be a bidentate five-membered-ring structure (like $GA_LH^+Li2^+/Na2^+$), the two $(C_{1,4})O-K^+$ bonds must be strong enough to conquer the torsion deformation of peptide chain and to compete against the stronger $(C_4)O...H(N_6)$ hydrogen-bonding (1.815 Å). Optimization reveals that there is no $K^+...O$ (C_4) bond formed in the $GA_LH^+K2^+$, i.e., only a monodentate ($(C_1)O-K^+$) structure is obtained due to no enough charge distribution over the K^+ to satisfy the bidentate coordination.

$GA_LH^+K1^+$ with a $(C_1)O-K^+$ bond is only 0.2 kcal/mol larger than $GA_LH^+K2^+$, thus the two complexes are very similar in stability. Interestingly, the bidentate $GA_LH^+Na2^+$ is higher in energy than monodentate AGH^+Na1^+ and becomes the second most stable structure. This may be attributable to the fact that the contribution of bidentate $Na^+...O(C_{1,4})$ is less than that of the repulsion from two positive charge centers in the $GA_LH^+Na2^+$ structure. Monodentate AGH^+Li1^+, however, is the second most stable complex. This perhaps ascribes to its largest H^+-Li^+ distance (6.635 Å) and least molecule dipole moment (9.9Debye) compared with other isomers (see Figure 1S and Table 1S of the Supporting Information). As a result, the least repulsion between two positive charge centers strengthens the stability of AGH^+Li1^+.

Due to a metal ion bound at the $(C_1)O$ site and a methyl linked close to the metal ion, the $GA_LH^+Li1^+$ and $GA_LH^+Na1^+$ become the third most stable structures among Li^+ and Na^+ involved complexes, respectively. It is noted that the linear GAH^+ could also be translated into L $GA_LH^+Li^+/Na^+$ after metalation (Li^+/Na^+) at the $(C_1)O$ site. As the metalation at the $(C_4)O$ site could lead to the shorter $H^+...M^+$ distance, stronger repulsion effect, and poorer structural stability, both $GAH^+M2'^+$ (Figure 1S) and AGH^+M2^+ are the poorest in stability. Table 1S shows that both of them have the largest dipole moments. A comparison reveals that the different space effects of the methyl in the two complexes result in the different distances of two positive charge centers and consequently different stability of the corresponding structure. For example, the distances in GAH^+Li2^+ and AGH^+Li2^+ are 3.593 Å and 3.619 Å, respectively, indicating that the latter will suffer less positive charge repulsion and have stronger stability. Relative energies confirm that AGH^+Li2^+ is 3.5 kcal/mol more stable than GAH^+Li2^+. Due to the poor $(C_4)O...K^+$ binding strength and probable stronger $K^+...H^+$ repulsion, no GAH^+K2^+ is obtained.

3.4. $AA_{(L)}H^+Mx^+$. As shown in Figure 2S of the Supporting Information, four metalated complexes $AA_{(L)}H^+Mx^+$ (i.e., $x = 1, 2$) are produced when two bare carboxyl oxygens of both AAH^+ and L AA_LH^+[5] react with M^+ (M = Li, Na, or K), respectively. As the alanine residue has an additional methyl than the glycine residue, the main chain rigidity of alanine-composed dipeptide would be much stronger, and accordingly, its metalated and protonated complexes would twist less. For example, the difference of $\tau(C_1C_2N_3C_4)$ angles of $AA_LH^+Mx^+$ and AAH^+Mx^+ is less than that of $GA_LH^+Mx^+$ and GAH^+Mx^+, or that of $GG_LH^+Mx^+$ and GGH^+Mx^+.

Similar to the $GA_{(L)}H^+Mx^+$ counterparts, the stability orders for $AA_{(L)}H^+Lix^+$ and $AA_{(L)}H^+Nax^+$ complexes (in kcal/mol) are $AA_LH^+Li2^+$ (0.0) > AAH^+Li1^+ (1.0) > $AA_LH^+Li1^+$ (6.3) > AAH^+Li2^+ (17.2) and AAH^+Na1^+ (0.0) > $AA_LH^+Na2^+$ (4.2) > $AA_LH^+Na1^+$ (5.8) > AAH^+Na2^+(16.2), respectively. Due to the lower charge distribution, K^+ cannot simultaneously coordinate with the two carboxyl oxygens of the $AA_{(L)}H^+$ to produce a bidentate structure, and thus the monodentate $AA_LH^+K1^+$ with $(C_1)O...K$ bonding is the most stable. $AA_LH^+K2^+$ could also degenerate into the monodentate $AA_LH^+K1^+$ and both of them have nearly similar stability (only 0.1 kcal/mol difference). To lessen the space repulsion caused by the methyl, AAH^+K1^+ must twist to some degree and finally hold the similar structure of $AA_LH^+K1^+$. Due to the shortest $K^+...H^+$ distance (4.160 Å), AAH^+K2^+ is the most unstable complex among its isomers.

3.5. GWH^+Mx^+. Relative energies show that GWH^+M2^+ is more stable because the metal ion is coordinated with both the carboxyl oxygen $(C_4)O$ of the glycine residue and a nitrogen of the indole ring (see Figure 3S of the Supporting Information). However, the energy of the complex will raise if the M^+ is bound at the $(C_1)O$ site.

3.5.1. Side-Chain and Metal-Ion Dependence of PBEs in These Different Complexes. The binding energies listed in Table 3 reveal that they are all positive (PBE), and changes with different side chains and different binding modes. It is interesting to note that the PBE order is opposite to the stability order of complex, i.e., the higher the PBE, the poorer the stability of the complex. For example, the energy of the $GG_LH^+Na2^+$ is 10.2 kcal/mol less than that of the GGH^+Na1^+ but 1.1 kcal/ mol more than that of $GG_LH^+Na1^+$, respectively. Its PBE differences compared with the latter two complexes are −9.9 and 1.5 kcal/mol accordingly, indicating a key role of PBE in their structure stability.

TABLE 3: Both ZPVE and BSSE-Corrected PBEs of These Protonated and Metalated Dipeptides from (I) B3LYP/6-31G*, and (II) B3LYP/6-311++G//6-31G*, Respectively[a]**

complex	I	II	complex	I	II	complex	I	II
$GG_LH^+Li2^+$	8.6	14.9	$GG_LH^+Na2^+$	23.6	29.2	$GG_LH^+K2^+$	25.2	26.7
$GG_LH^+Li1^+$	14.4	17.9	$GG_LH^+Na1^+$	24.3	27.7	$GG_LH^+K1^+$	31.2	32.8
GGH^+Li2^+	15.3	18.8	GGH^+Na2^+	24.5	27.8	GGH^+K2^+	30.9	32.6
GGH^+Li1^+	26.2	30.0	GGH^+Na1^+	35.5	39.1	GGH^+K1^+	41.2	43.2
$GA_LH^+Li2^+$	6.0	12.2	$GA_LH^+Na2^+$	21.4	26.9	$GA_LH^+K2^+$	25.1	26.6
AGH^+Li1^+	15.9	18.7	AGH^+Na1^+	25.9	28.6	AGH^+K1^+	32.8	33.9
GAH^+Li1^+	14.9	17.8	GAH^+Na1^+	25.2	28.0	GAH^+K1^+	32.5	33.4
$GA_LH^+Li1^+$	13.0	16.6	$GA_LH^+Na1^+$	23.4	26.8	$GA_LH^+K1^+$	25.2	26.8
AGH^+Li2^+	25.9	29.0	AGH^+Na2^+	35.6	38.6	AGH^+K2^+	41.8	43.1
GAH^+Li2^+	27.6	30.6	GAH^+Na2^+	37.1	40.1	$GAHK2^+$	–	–
$AA_LH^+Li2^+$	4.2	10.0	AAH^+Na1^+	19.2	21.9	$AA_LH^+K1^+$	24.7	25.8
AAH^+Li1^+	9.2	12.0	$AA_LH^+Na2^+$	19.9	25.0	AAH^+K1^+	26.5	27.4
$AA_LH^+Li1^+$	12.6	15.8	$AA_LH^+Na1^+$	23.1	26.2	$AA_LH^+K2^+$	24.8	25.9
AAH^+Li2^+	25.2	28.2	AAH^+Na2^+	35.2	38.2	AAH^+K2^+	41.6	43.0
$PG_LH^+Li2^+$	4.3	9.8	$PG_LH^+Na2^+$	20.4	25.2	$PG_LH^+K2^+$	24.4	25.2
PGH^+Li1^+	13.5	16.4	PGH^+Na1^+	23.7	26.4	PGH^+K1^+	31.2	32.0
$PG_LH^+Li1^+$	13.6	16.4	$PG_LH^+Na1^+$	23.8	26.4	$PG_LH^+K1^+$	30.3	31.5
PGH^+Li2^+	23.2	26.2	PGH^+Na2^+	33.1	36.1	PGH^+K2^+	39.6	40.9
GWH^+Li2^+	3.8	10.7	GWH^+Na1^+	19.6	22.6	GWH^+K1^+	27.3	28.4
GWH^+Li1^+	9.0	12.2	GWH^+Na2^+	21.3	27.5	GWH^+K2^+	33.7	36.4
			GSH^+Na1^+	22.9	25.4	GSH^+K1^+	30.3	31.1
			GTH^+Na1^+	19.9	22.8	GTH^+K1^+	23.2	24.5
			GFH^+Na1^+	19.0	22.1	GFH^+K1^+	27.0	28.3
			GYH^+Na1^+	18.0	21.3	GYH^+K1^+	26.3	27.7
			GVH^+Na1^+	17.2	19.5	GVH^+K1^+	24.8	25.5

[a] Energy in kcal/mol.

3.6. Side-Chain Effect on the PBE of the $P_2H^+Mx^+$ Complexes. In this section, because of the middle radii of Na^+ among the three M^+ ions and the geometrical similarity of P_2H^+-Nax^+ to $P_2H^+Lix^+$ and $P_2H^+Kx^+$ counterparts, only the P_2H^+-Nax^+ is taken as the model for convenience to explore the PBE changes with different side chains.

For the most stable complexes of $GG_LH^+Na2^+$ and GA_LH^+-$Na2^+$, they are distinct in structure in that the latter has one additional methyl. The methyl of the latter reduces its PBE by 2.3 kcal/mol relative to the former. When a methyl hydrogen of GAH^+Na1^+ is substituted by a much larger indole ring, the complex GWH^+Na1^+ would be produced and less PBE (5.4 kcal/mol) can be obtained relative to the former. This is the C_2-site substituted case. If the methyl is bound at the C_5 site, i.e., close to the amino terminal proton of GG_LH^+, then more PBE will be reduced (see Table 3). These results suggest that the $P_2H^+Mx^+$ with larger side chains generally has less PBE compared with those with smaller side chains. In fact, the PBE decrease with the increscent side chain can also be observed and confirmed from Kass' study[42] on the dianion systems.

Figure 4S shows the structures of $GSH^+Na1^+/K1^+$, GTH^+-$Na1^+/K1^+$, $GFH^+Na1^+/K1^+$, $GYH^+Na1^+/K1^+$, and GVH^+-$Na1^+/K1^+$, respectively. It should be noted that the five optimized dipeptides are initially designed by consulting the linear GAH^+M1^+ structure so that their PBE comparisons can avoid the intervention of deformation factors. Thus, these dipeptides may not always correspond to each global minimum on their PESs, but at least one local minimum. Taking into account the carbonyl oxygens of each TVGYG chain lining in the KcsA K^+ channel,[19] the linear and *no other shape of* GAH^+M1^+ *structure* is regarded as a template to construct initial $GSH^+Na1^+/K1^+$, $GTH^+Na1^+/K1^+$, $GFH^+Na1^+/K1^+$, GYH^+-$Na1^+/K1^+$, and $GVH^+Na1^+/K1^+$, and thus no global minimum of each complex is searched for fastidiously. In fact, following MD-simulations on model 1 also revealed that the structures of these dipeptide sections are always altering along the ion transport in order to acclimatize themselves to new states.

The PBE values of these dipeptides in Table 3 (see Figure 4S) reveal that larger side chains will reduce more PBE and favor M^+-O bonding. Interestingly, larger side chains in Table 3, such as $-CH_2-C_5H_5$, not only lower PBE but also compel the bare carbonyl oxygens to locate on the same side of the main chain (see GWH^+M1^+ in Figure 3S and GFH^+M1^+ in Figure 4S of the Supporting Information). This would favor the ion transport in a channel.[19]

The two carbonyl oxygens in $GVH^+Na1^+/K1^+$ locate at the same side of the main chain, like the case of $GTH^+Na1^+/K1^+$. Calculations suggest that the PBE of GVH^+Na1^+ (19.5 kcal/mol) is less than that of GTH^+Na1^+ (22.8 kcal/mol), whereas the PBE value (25.5 kcal/mol) of GVH^+K1^+ is more than that of GTH^+K1^+ (24.5 kcal/mol). As their side chains are $-CH(CH_3)_2$ and $-CH(CH_3)OH$, respectively, these PBE data indicate that the methyl group is more favorable to the Na^+-O bonding than a hydroxyl, but unfavorable to the K^+-O bonding. The phenomenon would be important in understanding the ion selectivity in the K^+ channel protein.[30]

3.7. Metal Ion Effect on the PBE of the $P_2H^+Mx^+$ Complexes. For the M^+-involved systems, the PBE generally increases with the enlargement of M^+ radius. For example, the PBEs of $GG_LH^+Li1^+$, $GG_LH^+Na1^+$, and $GG_LH^+K1^+$ are 17.9, 27.7, and 32.8 kcal/mol, respectively. Table 3 reveals that the PBE of any Li^+ ion-involved system is less, by about 10.0 kcal/mol, than that of their Na^+ involved counterpart, indicating the stronger binding ability of Li^+. When compared with K^+-involved system, the PBE of its Na^+-involved counterpart is also smaller, though their PBE difference is not obvious. However, there are still some exceptions observed. For example, the PBE of $GG_LH^+Na2^+$ (29.2) is larger than that of GG_LH^+-$K2^+$ by 26.7 kcal/mol. Further investigation found that such abnormalities are caused by the monodentate bonding and less electrostatic repulsion (longer H^+-K^+ distance) in the GG_LH^+-$K2^+$ complex.

3.7.1. Pertinence between Different Side Chains, PBEs and Biological Phenomena. In a transmembrane ion channel, a key factor to determine ion selectivity is the binding strength between the ion and the active site of the ligand.[33] Thus, the dependence of PBEs on the side chains of these dipetides can be employed to illuminate the reason why the different amino

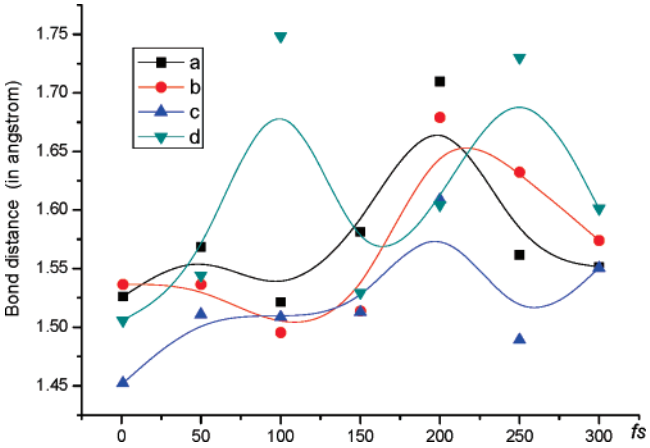

Figure 2. Distances of four side chains along ions transport time in a K^+ channel selectivity filter.

acids of four TVGYG chains are strictly conserved in the KcsA K^+ channel protein.[19]

3.8. Side-Chain Effect in the KcsA K^+ Channel. The distances of Y side chains ($R_1 = -CH_2-C_5H_5$) in the four TVGYG residue chains are defined as a_i ($i = 1$, 2, 3, and 4) (see Scheme 1, in which only two opposite TVGYG residue chains ($i = 1$ and 2) are shown for succinctness), where a denotes the average distance of a_1, a_2, a_3, and a_4. The distances of four V side chains ($R_2 = -CH(CH_3)_2$) refer to the b_i, and b is also the average distance of four b_i. The variables c and d are also the average distances of amido ($R_3 = -NH_3$) and methyl ($R_4 = -CH_3$) side chains in four T residues, respectively. Simulation reveals that the PES of the system has trended to a constant less than 1000 fs, and at the 300 fs, top K^+ ion in the corresponding structure is disengaging from the system (see Figure 5S of the Supporting Information). Thus, only the changes of the four average distances (a, b, c, and d) along the simulation times of less than 300 fs are selected, and among them, only those corresponding to seven equidistant time points (0, 50, 100, 150, 200, 250, and 300 fs) are depicted in Figure 2. The first time point (0 fs) corresponds to the initial model structure drawn directly from the PDB file 1bl8.[19,36] The energy changes of the seven corresponding model structures are shown in Figure 3.

Figure 2 reveals that the distances of all side chains are continuously altering in the ion transport process and the ion transport favors the stability of the system in general (see also Figure 3). The energies of the system relate nearly to the changes of a, b, c, and d. For example, at 100 fs when the system corresponds to a local minimum, the distances (a, b, c) of three larger side chains change slightly relative to those in the initial structure at 0 fs. Moreover, only at 200 fs, the values of a, b, and c change significantly. The d value, however, changes obviously in the following six time-point (50, 100, 150, 200, 250, and 300 fs) model structures, especially in the 100- and 250-fs structures relative to that in the initial 0-*fs* structure, indicating that the smallest side chain (R_4) suffers the strongest electrostatic repulsion and thus the most serious distance (d) change in the process of ion transport. The phenomenon is consistent with the case of GAH^+K1^+ (with R_4 side chain), whose side chain is in the smallest size but has the largest (33.4 kcal/mol) PBE compared with GYH^+K1^+, GVH^+K1^+, GTH^+K1^+, which have larger side chains R_1, R_2, and R_3, respectively. On the basis of the above description, we are not surprised to find that the GGH^+K1^+ with no side chain has much more PBE (43.2 kcal/mol) than those species with side chains such as GAH^+K1^+ (33.4 kcal/mol) and GSH^+K1^+ (31.1 kcal/mol) (GSH^+K1^+ can be obtained by substituting hydroxyl for methylic hydrogen of GAH^+K1^+). Since the larger PBE could facilitate the ion transport,[19] the above data also explain the reason why a single-point mutation, Ser-68 to glycine, is sufficient to restore K^+ permeability to AtHKT1, and the reverse mutation in HKT1, Gly-91 to serine, abrogates K^+ permeability.[43]

Figure 5S of the Supporting Information lists the structures of seven time points and their corresponding electrostatic potential (EP, in crimson) of the four-residue model (model 1) and two-residue model (model 2). The figure reveals that the EP always locates at the T residue, which has two small-sized side chains, R_3 and R_4. Such a phenomenon conforms to our above analysis on the relationship between the side-chain size and the PBE or electrostatic repulsion. The larger EP isovalue differences between model 1 (1.6×10^{-6}) and model 2 (1.6×10^{-4}) indicate that the multicoordination for a K^+ ion can greatly decrease their EPs. More significantly, Figure 5S reveals that the escape of a K^+ ion from the model 2 channel needs less than 300 fs; however, the transport rates in the two models are almost equal. Thus, with the exception of PBE, the EP may be another important factor that can influence the ion transport. Our previous study[25a] confirmed that the multi-coordination of K^+ could decrease more PBE than its oligo-coordination state and thereby would strengthen the attractive force between the K^+ and the ligand.

3.9. Breathing Motion in the Selectivity Filter. The distances r_i ($i = 1$, 2, 3, and 4) shown in Scheme 1 and Figure 4 refer to the average distance of two pairs of opposite carboxyl oxygens of each kind of amino acid residue in the selectivity filter; r_5 denotes the average distance of two pairs of opposite hydroxyl oxygens in four T residues. These average distances can also be approximately regarded as the pore diameter of the selectivity filter.

From Figure 4, we can see that the distances of r_3 and r_4 at the initial state (0 fs) are 4.700 and 5.475 Å, respectively. There are two K^+ ions coordinating, respectively, two adjacent positions, S4 and S5, thus larger EP should be there. Although there are a few fluctuations from 50 fs to 300 fs, the r_3 and r_4 generally become shorter during the ion transport process and do not deviate too obviously from its initial state (0 fs). It can be expected that the shortened r_3 and r_4 would lead to the increment of EPs. In fact, such prediction is confirmed by Figure 5S of the Supporting Information, in which one can see that the most EPs are borne by the T residue and the c and d values of T residues elongate more obviously. This indicates that the VT motif of the main chain of these peptides basically keeps stable and the electrostatic repulsion from two K^+ ions can be absorbed by their side chains (R_2, R_3, R_4). If the K^+ ion at the S5 position is absent and the model system becomes the more stable configuration[44] with S2 and S4 occupied by ions and S3 occupied by a water molecule, as well as empty S5, then where should the larger EP be located? Computations (not listed in this work) show that the EP still locates at the side chains of T. This indicates that the T residue plays an "electrostatic buffer" role in the selectivity filter due to its unique location, and the EPs mainly distribute at the methyl (R_3) and amido (R_4) groups of residues T. From 100 to 150 fs, r_5 keeps the largest value, indicating that this time span is optimal for the water to influx from the cavity to selectivity filter due to its larger volume than K^+.

The remarkable changes can be observed from r_2. As shown in Scheme 1, the distance r_2 refers to the average distance between two opposite carboxyl oxygens of two pairs of glycine

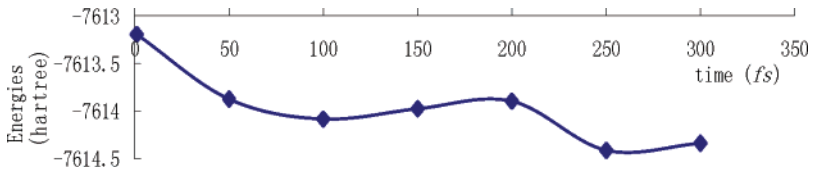

Figure 3. Engergy changes along the simulation time.

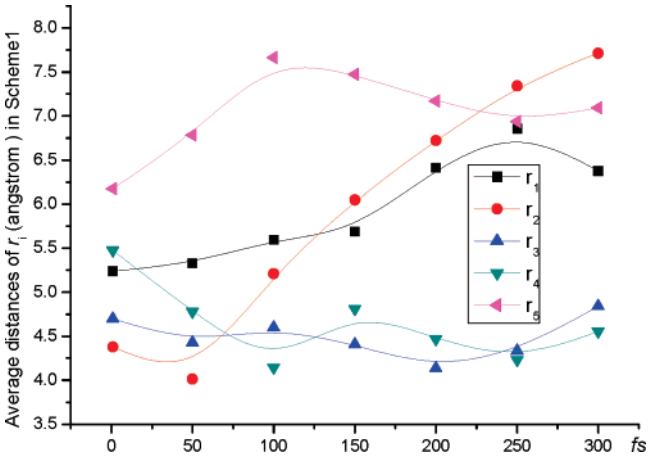

Figure 4. Average distance changes of two opposite carboxyl oxygens (r_1-r_4) and hydroxyl oxygens (r_5) along with the simulation time.

residues. Figure 4 reveals that the r_2 of initial structure (0 fs) is the shortest,[19] but it nearly increases monotonously along with the ions transport before the K^+ ion escapes from the filter mouth. This further confirms the above fact that the PBE of GGH^+K1^+ is larger than any other complexes with side chains, such as GYH^+K1^+, GVH^+K1^+, GTH^+K1^+, and so forth, and is also in good accordance with the observation that the selectivity of the channel for K^+ is mediated by those filter glycines and by electrostatic interactions inside the filter.[45] Thus, the ion coordination at the carboxyl oxygens of G residues in model 1 would lead to a larger electrostatic repulsion and a stronger deformation (or extension) of the peptide main chain. The case is different from the ion coordination at the carboxyl oxygens of other three amino acid residues (T, V, and Y) with side chains.

Y residue locates between the two G residues in the TVGYG chain, so r_1 would be affected by these two G neighbors. The calculation reveals that r_1 has a minor increase along with the ion transport, and the changes of r_1 mainly derive from the displacement of the carboxyl oxygen of a Y residue. In such a case, the carboxyl oxygen is moved out from the inside of the selectivity filter. It may be that the deformation becomes smaller after the first G (left out in model 1 for simplified computation) is taken into account. It is unquestionable that in any case, the r_1 changes less than r_2. This further confirms that the side chains of T, V, and Y not only bear electrostatic interactions, but also keep the corresponding main chain segments less deformed.

Considering the changes of side-chain lengths (a_i) mentioned above, we can expect that the remarkable "breathing motion"[28] may mainly take place at the two G residue locations, because the main chains of G-composed peptides are flexible enough to achieve the optimal K^+ coordination structures. The other three residues with side chains keep fewer changes, i.e., minimize their flexibility along with the ion transport. Analyses also reveal that the smaller side chain will extend from the main chain more obviously and bear more EPs than the larger one because larger side chains can maximize their own rigidity and their parental residues in the main chains. The results are consistent with our above PBE analysis and the observation of Ban et al.[30]

3.10. Function of T Residues in the Selectivity Filter. The locations of the four T residues are all at the end of the selectivity filter, in which K^+ or water molecules (W) can pass from the cavity to selectivity filter.[19] Different from V, G, and Y, the T side chain is characterized by hydroxyl group (−OH), and the four -OH groups just locate at the forefront of the filter. Besides acting as the "EP buffer" (see above section), the T residues also play important roles in controlling the water to influx into the filter.

Figure 5 sketches the conditions of water-molecule permeation into the selectivity filter through the hydroxyl groups of the four T residues. In Figure 5A, for simplification, the four T residues are represented by four −OH, respectively. Figure 4 shows that the r_5 distance is between 6.173 and 7.663 Å. Such a larger r_5 will favor the water molecule influx. From Figure 5B, one can see that the distance between the two H_2O molecules in the most stable dimer (2W) is 2.778 Å, and the affinity energy of this optimal dimer (compared with two isolate H_2O molecules) is calculated to be 3.2 kcal/mol. Further separation between the two H_2O molecules would decrease its stability; and, at about 4.0 Å, the dimer begins to dissociate into two separate water molecules.

In the cavity of the cellular membrane, there are large numbers of water molecules. The influx of a water molecule into the selectivity filter from the cavity must overcome the affinity interactions of other water-molecule clusters and of the hydroxyls of four T residues first. Another factor affecting the influx is the distance between two opposite hydroxyls (r_5), which can roughly represent the "mouth space" of the selectivity filter. Shorter r_5 will keep the water molecules outside of the filter and only allow the K^+ influx. In addition, as shown in Figure 5A, the electrostatic interaction of the K^+ with the water molecule would be an important driving force for the water molecule influx into the filter.

The water clusters constituted by two (2W), three (3W), four (4W), and five (5W) water molecules, together with the monohydrated K^+ (KW), are shown in Figure 5C. The affinity energies between a water molecule and the remainder part in these hydrates are listed in Figure 5D. From Figure 5D, we can observe that the 4W has the largest affinity energy compared with 2W, 3W, and 5W clusters. In fact, we obtain two tetrahydrated clusters, 4W and 4W1, and each of them has one four-membered-ring structure. However, because the difference of their affinity energies is as small as 0.6 kcal/mol, only the affinity energy of 4W is depicted in Figure 5D. From Figure 5C, one can find that the three oxygens linked by three H bonds in 3W are right coplanar, and the four oxygens in 4W also display the shape of plane but with slight distortions ($\angle O_1O_2O_3O_4 = 5.4°$). The linkages between two water molecules in the two clusters are their hydrogen bonds. These hydrogen bonds are also almost in the planes constituted by these oxygens. The largest distances between two water molecules in 2W, 3W, and 4W are 3.663, 3.870, and 4.777 Å, respectively. The hydrogen-bonding distances in these clusters are 2.029∼2.245, 1.822∼1.840,

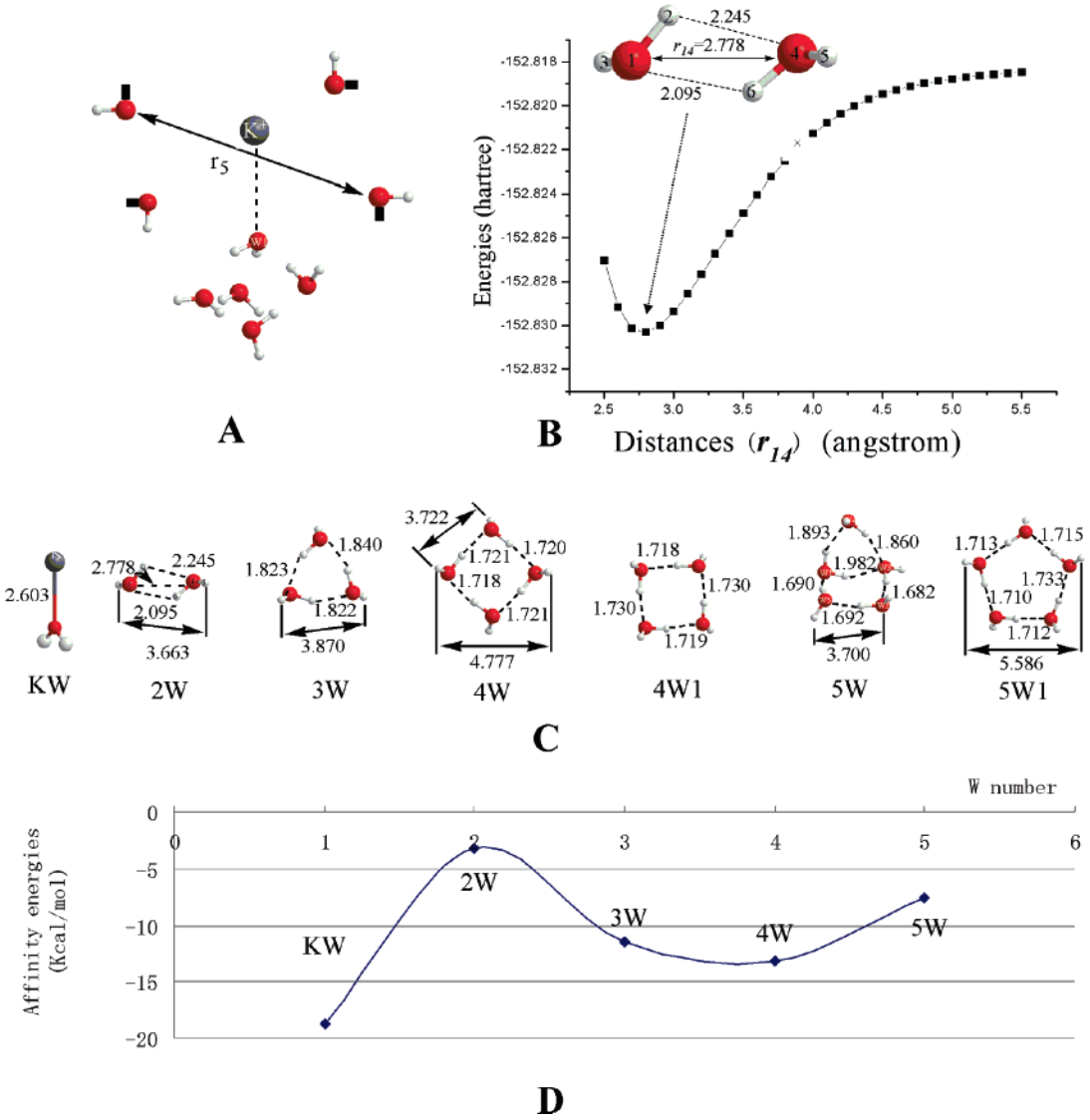

Figure 5. Illustration on the function of four hydroxyls of the T residues in the selectivity filter. (A) The sketch of four hydroxyls of the T residues. r_5 is the same as that in Scheme 1 and a water molecule (W_1) of 5W is entering the cavity composed of the four hydroxyls. In the cavity, a K^+ has been embedded. (B) The PES of a water (W) dimer along their contact distance between two oxygens. (C) Structures of 2W, 3W, two 4Ws, and two 5Ws, as well as a KW. Distances are in angstroms. (D) The affinity energies of a water molecule in KW, 2W,..., and 5W, respectively.

and 1.718∼1.730 Å, respectively. This gradual decreasing trend of H-bond length from 2W to 4W is in agreement well with the increasing trend of affinity strength. For 5W, optimization reveals that its five oxygen atoms are no longer in-plane, which can be regarded as the combination of a "3W" planar unit with another "4W" planar unit (the angle between the two planes is about 108.0°), bridged by an O−H−O chain between the W1 and W3 water molecules (see 5W in Figure 5C). The dihedral angle of four oxygens of "4W" unit in 5W has extended to 12.5°, larger than that in 4W species. The affinity energy of 5W per H_2O molecule is −7.5∼−8.1 kcal/mol, smaller than that of 4W. In addition, 5W1, which is the isomer of 5W and has a five-membered-ring, is also found by our calculations. When compared with 5W, the 5W1 is more stable by 4.7 kcal/ mol, and its affinity energy per water molecule is also larger by 4.6 kcal/mol. This indicates that the dehydration of a water molecule from 5W1 is more difficult than that from 5W. What about the 6W cluster (made of six H_2O molecules) with a six-membered-ring structure (not displayed in Figure 5C)? Calculations reveal that it has 14.2 kcal/mol affinity energy, implying the greater difficulty for 6W to dehydrate. Thus, in combination with the shorter distance between two water molecules (3.700 Å) and weaker affinity of a water molecule in 5W than in 5W1, the 5W cluster may be a more suitable water donor in the cavity to influx into the filter (Figure 5A).

The distance (r_5) of two hydroxyls in T residues is long enough for a single water molecule to influx into the filter. The H bonding interaction between the H_2O molecule and any −OH group of T residues is very weak because the distance of $(H_2O)O...H(-OH)$ is much longer than the distance of $(H_2O)O...H(H_2O)$ in 2W, 3W, 4W, and 5W. Figure 5B confirms that the affinity energy decreases rapidly with the increment of $(H_2O)O...O(H_2O)$ distance for the 2W cluster. The weaker affinity energy is 7.7 kcal/mol in 5W. The solvation free energy of K^+ is −84.1 kcal/ mol,[47] and the largest coordination number in the filter[30] as well as most hydrated number for the K^+ is eight.[42a] Thus, the average binding energy of each K^+−O bond is about −10.5 kcal/mol, larger than the affinity energy (such as 7.7 kcal/mol in 5W) of the water molecule got from the solution in cavity and hydroxyls in T residues. Weaker affinity would favor one water molecule to disengage from those two- or multi-hydrated clusters in the outer cavity to influx into the filter conveniently. Therefore, one water molecule can be loaded

in the selectivity filter by the interacting force of K^+ locating at the S5 site, which can be clearly seen in Figure 5A.

Now we begin to explore the case of two water molecules entering the filter. Due to the initial r_5 distance of ~6 Å in the filter,[36] we could expect that the minimum W−W distance of the two water molecules (one two-water unit) in the multihydrated clusters should also match this r_5 in order to infiltrate into the filter. According to our above calculations, the minimum W−W distance of one two-water unit can be estimated as $2 \times 1.682 + 3.700 = 7.064$ Å, where 1.682 and 3.700 are the H-bond length and W−W distance in 5W, respectively, both of them being the shortest ones compared with those of 3W, 4W, 4W1, and 5W1 species (Figure 5C). It should be mentioned that although the W−W distance in 2W cluster (3.663 Å) is even shorter, it is not adopted here because the formation of multihydrated clusters is much more probable than the formation of 2W clusters in the cavity. Because the estimated distance (7.064 Å) is larger than r_5 (6 Å), we can expect that the initial state of selectivity filter may not have enough space to accommodate the two-water unit entering into its inner space, with the exception of some special time span, such as 100−150 fs (see r_5 in Figure 4). In addition, because the affinity energies of the water dimer in the 4W, 5W, 5W1, and 6W clusters are −23.0, −18.1, −23.1, and −16.3 kcal/mol, respectively, one two-water unit influx into the filter is also difficult. At last, the K^+−O binding energy of the monohydrated (KW) cluster is −18.8 kcal/mol in ref 46 (our value is −18.7 kcal/mol), whereas that of the hexahydrated K^+ cluster has decreased to −14.7 kcal/mol,[46] indicating that the K^+ locating at the S5 site of the selectivity filter cannot induce a two-water unit into its inner place. Thus, we can conclude that the accommodation of one two-water unit into the filter is very difficult unless assisted by plenty of energy from other resources.

3.11. Ion Selectivity in the Selectivity Filter. As shown in Table 3, the PBE difference between GGH^+K1^+ and GGH^+Na1^+ and that between GTH^+K1^+ and GTH^+Na1^+ are 4.1 and 1.7 kcal/mol, respectively; the difference between GYH^+K1^+ and GYH^+Na1^+ and that between GVH^+K1^+ and GVH^+Na1^+ are 6.4 and 6.0 kcal/mol, respectively. Larger PBE difference implies the larger attractive force of Na^+ than K^+. The balance between the attraction of one K^+ with filter and the repulsion with its adjacent K^+ would be the bottom-most condition to allow K^+ transport into the filter.[19] Obviously, the repulsion force from the K^+ ions in the selectivity filter might be the driving force of K^+ ion transport, albeit locally unfavorable for the stability of the system.[26] In view of the PBE, the Y and V residues should be determinative for the K^+ highly selectivity over Na^+ in the filter because the less PBE differences between GGH^+K1^+ and GGH^+Na1^+ (4.1 kcal/ mol,) and between GTH^+K1^+ and GTH^+Na1^+ (1.7 kcal/mol). Our previous studies[25] revealed that a larger distance between two different ions in the peptide would make its PBE a negative one[26] and disfavor the ion transport. Thereby, the transport of ions and intervenient water should occur in a concerted manner[48] in point of binding energy property. It may be that only one single water molecule is suitable to accompany the two K^+ ions transport because, if there are two adjacent water molecules between them, then it would separate two K^+ ions far enough to have negative K^+−O binding energy in the filter. Figure 4S of the Supporting Information shows that the K^+−O orientation in GTH^+K1^+ is altered seriously relative to the Na^+−O orientation in GTH^+Na1^+, very different from those in any other protonated and metalated dipeptides. This further verifies that the T residue plays an important role in the Na^+/K^+ selectivity.

4. Conclusions

The metalated and protonated dipeptide derivatives, $GGHM x^+$, $GAH^+M x^+$, $AGH^+M x^+$, $AAH^+M x^+$, and $GWH^+M x^+$ ($x = 1, 2$; M = Li, Na, K), are investigated at the B3LYP/6-311++G**// B3LYP/6-31G* level, and the most stable structure is found to be the $P_2H^+M1^+$, due to the long distance between H^+ and $M1^+$, which induces the least electrostatic repulsion in the complex. Calculations reveal that the greater the PBE of a complex becomes, the poorer its stability will be; and the larger the side chain, the smaller the PBE. The larger the ion radius becomes, the greater the PBE will be in the similar structure generally.

The two G residues in the TVGYG chains are the most flexible positions, in which the serious deformation of the main chains can be observed when K^+ ions transport through the filter. The deformation mainly derives from the strong electrostatic repulsion of two adjacent K^+ ions and the repulsion occurring at the two G positions can be released only by the larger deformation of the two G residues. For the other three residues, T, V, and Y, however, the repulsion can be also released via their side chains. Calculations reveal that the entire EPs of the filter model mainly locate at the T residues and the amido side chain is the primary carrier of the EPs. The larger distance (>6 Å) of two opposite hydroxyl oxygens (r_5) in the T residues favors one water molecule entry, but is insufficient for two or even more water molecules to enter together. For the r_3 and r_4, less change would favor the K^+-dehydration and K^+-transport (Scheme 1 and Figure 4). The unique structure of T not only helps a K^+ ion or a water molecule penetrate into the filter from the outer cavity, but also keeps them from being conjoint during ion transport within the filter. V residues will further separate them into two different sites (see S3, S4, etc., in Scheme 1) in the filter and keep the filter structure with fewer changes with its larger side chains (R_2). The Y can cushion stronger electrostatic repulsion, which derives from the two neighboring K^+ ions located at the fore-and-aft G residues. With respect to K^+, its larger ion radius (compared with Li^+ or Na^+ ion) and its larger PBE favor its transport into the filter.

Acknowledgment. H. Ai gratefully acknowledges the support of NSFC(20573047) and the Foundation for Doctoral Start-up by University of Jinan (B0418, B0302). This work is partially supported by the Key Subject Research Foundation of Shandong Province XTD 0705.

Supporting Information Available: The dipole moments (Debye) of these $GA_{(L)}H^+Nax^+$ and AGH^+Nax^+ dipeptides are shown in Table 1S. The geometries of $GA_{(L)}H^+Mx^+$ and $AG_{(L)}H^+Mx^+$, $AA_{(L)}H^+Mx^+$, GWH^+Mx^+, and GFH^+M1^+, GSH^+M1^+, GTH^+M1^+, GYH^+M1^+, and GVH^+M1^+, respectively, are shown in Figures 1S−4S. Seven states of the models (1, 2) including three K^+ ions and a water molecule taken at 0, 50, ..., 300 fs, respectively, are shown in Figure 5S. This material is available free of charge via the Internet at http://pubs.acs.org.

References and Notes

(1) Strittmatter, E. F.; Williams, E. R. *Int. J. Mass Spectrom.* **1999**, *185/186/ 187*, 935.

(2) Zhang, K.; Cassady, C. J.; Chung-Phillips, A. *J. Am. Chem. Soc.* **1994**, *116*, 11512.

(3) Paizs, B.; Csonka, L. P.; Lendvay, G.; Suhai, S. *Rapid Commun. Mass Spectrom.* **2001**, *15*, 637.

(4) Rodriquez, C. F.; Cunje, A.; Shoeih, T.; Chu, I. K.; Hopkinson, A. C.; Michael Siu, K. W. *J. Am. Soc. Chem.* **2001**, *123*, 3006.

(5) Kohtani, M.; Breaux, G. A.; Jarrold.; M. F. *J. Am. Soc. Chem*. **2004**, *126*, 1206.

(6) Wyttembach, T.; Bushnell, J. E.; Bowers, M. T. *J. Am. Chem. Soc.* **1998**, *120*, 5098.

(7) (a) Jensen, F. *J. Am. Chem. Soc.* **1992**, *114*, 9533. (b) Hoyau, S.; Ohanessian, G. *Chem. Eur. J.* **1998**, *4*, 1561; Hoyau, S.; Ohanessian, G. *J. Am. Chem. Soc.* **1997**, *119*, 2016. (c) Ai, H.; Bu, Y.; Han, K. *J. Chem. Phys.* **2003**, *118*, 10973.

(8) Cox, H. A.; Julian, R. R.; Lee, S. W.; Beauchamp, J. L. *J. Am. Chem. Soc.* **2004**, *126*, 6485.

(9) Kohtani, M.; Jarrold, M .F.; Wee, S.; O'Hair, R. A. J. *J. Phys. Chem. B.* **2004**, *108*, 6093.

(10) Benzakour, M.; Mcharfi, M.; Cartier, A.; Daoudi, A. *J. Mol. Struct. (THEOCHEM*) **2004**, *710*, 169.

(11) Benzakour, M.; Cartier, A.; Mcharfi, M.; Daoudi, A. *J. Mol. Struct.* (*THEOCHEM*) **2004**, *681*, 99.

(12) Kapota, C.; Lemaire, J.; Maître, P.; Ohanessian, G. *J. Am. Chem. Soc.* **2004**, *126*, 1836.

(13) Kish, M. M.; Wesdemiotis, C.; Ohanessian, G. *J. Phys. Chem. B* **2004**, *108*, 3086.

(14) Kish, M. M.; Ohanessian, G.; Wesdemiotis, C. *Int. J. Mass Spectrom.* **2003**, *227*, 509.

(15) Cerda, B. A.; Hoyau, S.; Ohanessian, G.; Wesdemiotis, C. *J. Am. Chem. Soc.* **1998**, *120*, 2437.

(16) Kulhánek, P.; Schlag, E. W.; Koča, J. *J. Am. Chem. Soc.* **2003**, *125*, 13678.

(17) (a) Birge, R. R.; Govender, D. S. K.; Lzgi, K. C.; Tan, E. H. L. *J. Phys. Chem.* **1996**, *100*, 9990. (b) Palmgren, M. G.; Buch-pedersen, M. J.; MØller, A. L. *Ann. N. Y. Acad. Sci.* **2003**, *986*, 188.

(18) (a) HÅkansson, K. O.; Jorgensen, P. L. *Ann. N. Y. Acad. Sci.* **2003**, *986*, 163. (b) Jorgensen, P. L. *Ann. N. Y. Acad. Sci.* **2003**, *986*, 22.

(19) Doyle, D. A.; Cabral, J. M.; Pfuetzner, R. A.; Kuo, A. L.; Gulbis, J. M.; Cohen, S. L.; Chait, B. T.; MacKinnon, R. *Science* **1998**, *280*, 69.

(20) Shields, S. J.; Bluhm, B. K.; Russell, D. H. *J. Am. Soc. Mass Spectrom.* **2000**, *11*, 626.

(21) Yu, X.; Hao, L.; Inesi, G. *J. Biol. Chem*. **1994**, *269*, 16656.

(22) Ai, H.; Bu, Y.; Han, K. *J. Chem. Phys.* **2002**, *117*, 7593.

(23) Ai, H.; Bu, Y.; Chen, Z. *J. Chem. Phys.* **2003**, *118*, 1761.

(24) Ai, H.; Bu, Y. *J. Chem. Phys.* **2004**, *120*, 2208.

(25) (a) Ai, H.; Bu, Y.; Li, P.; Yan, S. *J. Chem. Phys.* **2005**, *123*, 134307. (b) Ai, H.; Li, Y.; Zhang, C.; Feng, J. *Chem. Phys.* **2007**, *334*, 64.

(26) Guidoni, L.; Torre, V.; Caloni, P. *FEBS Lett.* **2000**, *477*, 37.

(27) Sugita, Y.; Miyashita, N.; Ikeguchi, M.; Kidera, A.; Toyoshima, C. *J. Am. Chem. Soc.* **2005**, *127*, 6150.

(28) Shrivastava, I. H.; Sansom, M. S. *Biophys. J.* **2000**, *78*, 557.

(29) MacKinnon, R.; Cohen, S. L.; Kuo, A. L.; Lee, A.; Chait, B. T. *Science* **1998**, *280*, 106.

(30) Ban, F.; Kusalik, P.; Weaver, D. F. *J. Am. Chem. Soc.* **2004**, *126*, 4711.

(31) Bertran, J.; Sautiago, L. R.; Sodupe, M. *J. Phys. Chem. B.* **1999**, *103*, 2310.

(32) (a) Rodriquez, C. F.; Cunje, A.; Shoeib, T.; Chu, I. K.; Hopkinson, A. C.; Michael Siu, K. W. *J. Am. Chem. Soc.* **2001**, *123*, 3006. (b) Balta, B.; Basma, M.; Aviyente, V.; Zhu, C.; Lifshitz, C. *Int. J. Mass Spectrom.* **2001**, *201*, 69.

(33) (a) Becke, A. D. *J. Chem. Phys.* **1993**, *78*, 5648. (b) Becke, A. D. *Phys. Rev. A.* **1998**, *38*, 3098. (c) Lee, C.; Yang, W.; Parr, R. G. *Phys. Rev. B.* **1988**, *37*, 785. (e) Vosko, S. H.; Wilk, L.; Nusair, M. *Can. J. Phys.* **1980**, *58*, 1200.

(34) Boys, S. F.; Bermardi, F. *Mol. Phys.* **1970**, *19*, 553.

(35) Frisch, M. J.; Trucks, G. W.; Schlegel, H. B.; Scuseria, G. E.; Robb, M. A.; Cheeseman, J. R.; Montgomery, J. A., Jr.; Vreven, T.; Kudin, K. N.; Burant, J. C.; Millam, J. M.; Iyengar, S. S.; Tomasi, J.; Barone, V.; Mennucci, B.; Cossi, M.; Scalmani, G.; Rega, N.; Petersson, G. A.; Nakatsuji, H.; Hada, M.; Ehara, M.; Toyota, K.; Fukuda, R.; Hasegawa, J.; Ishida, M.; Nakajima, T.; Honda, Y.; Kitao, O.; Nakai, H.; Klene, M.; Li, X.; Knox, J. E.; Hratchian, H. P.; Cross, J. B.; Adamo, C.; Jaramillo, J.; Gomperts, R.; Stratmann, R. E.; Yazyev, O.; Austin, A. J.; Cammi, R.; Pomelli, C.; Ochterski, J. W.; Ayala, P. Y.; Morokuma, K.; Voth, G. A.; Salvador, P.; Dannenberg, J. J.; Zakrzewski, V. G.; Dapprich, S.; Daniels, A. D.; Strain, M. C.; Farkas, O.; Malick, D. K.; Rabuck, A. D.; Raghavachari, K.; Foresman, J. B.; Ortiz, J. V.; Cui, Q.; Baboul, A. G.; Clifford, S.; Cioslowski, J.; Stefanov, B. B.; Liu, G.; Liashenko, A.; Piskorz, P.; Komaromi, I.; Martin, R. L.; Fox, D. J.; Keith, T.; Al-Laham, M. A.; Peng, C. Y.; Nanayakkara, A.; Challacombe, M.; Gill, P. M. W.; Johnson, B.; Chen, W.; Wong, M. W.; Gonzalez, C.; Pople, J. A. *Gaussian 03*, Revision C.02, Gaussian, Inc., Wallingford CT 2004.

(36) (a) Sussman, J. L.; Lin, D.; Jiang, J.; Manning, N. O.; Prilusky, J.; Ritter, O.; Abola, E. E. *Acta Cryst. D* **1998**, *54*, 1078. (b) Abola, E. E.; Sussman, J. L.; Prilusky, J.; Manning, N. O. *Methods Enzymol.* **1997**, *277*, 556.

(37) Compoint, M.; Ramseyer, C.; Huetz, P. *Chem. Phys. Lett.* **2004**, *397*, 510.

(38) Perdew, J. P.; Wang, Y. *Phys. Rev. B* **1992**, *45*, 13244.

(39) Delley, B. *J. Chem. Phys.* **2000**, *113*, 7756.

(40) Tsukamoto, T.; Ishikawa, Y.; Vilkas, M. J.; Natsume, T.; Dedachi, K.; Kurita, N. *Chem. Phys. Lett.* **2006**, *429*, 563.

(41) Wakisaka, A.; Watanabe, Y. *J. Phys. Chem. B.* **2002**, *106*, 899.

(42) Kass, S. R. *J. Am. Chem. Soc.* **2005**, *127*, 13098.

(43) Mäser, P.; Hosoo, Y.; Goshima, S.; Horie, T.; Eckelman, B.; Yamada, K.; Yoshida, K.; Bakker, E. P.; Shinmyo, A.; Oiki, S.; Schroeder, J. I.; Uozumi, N. *PNAS* **2002**, *99*, 6428.

(44) Aqvist, J.; Luzhkov, V. *Nature* **2000**, *404*, 881.

(45) (a) Zhou, Y. F.; Morais, Cabral, J. H.; Kaufmar, A.; MacKinnon, R. *Nature (London*) **2001**, *414*, 43. (b) Nakamura, R. L.; Anderson, J. A.; Gaber, R. F. *J. Biol. Chem.* **1997**, *272*, 1011. (c) Roux, B.; MacKinnon, R. *Science* **1999**, *285*, 100. (d) Bemeche, S.; Roux, B. *Nature (London*) **2001**, *414*, 73.

(46) Glendening, E. D.; Feller, D. *J. Phys. Chem.* **1995**, *99*, 3060.

(47) Tissandier, M. D.; Cowen, K. A.; Feng, W. Y.; Gundlach, E.; Cohen, M. H.; Earhart, A. D.; Tuttle, T. R.; Coe, J. V. *J. Phys. Chem. A.* **1998**, *102*, 9308.

(48) Morais Cabral, J. H.; Zhou, Y.; MacKinnon, R. *Nature (London*) **2001**, *414*, 37.